

Supporting information for:

Post-synthetic Halide Conversion and Selective Halogen Capture in Hybrid Perovskites

Diego Solis-Ibarra, Ian C. Smith, and Hemamala I. Karunadasa *

Department of Chemistry, Stanford University, Stanford, California 94305, United States

*hemamala@stanford.edu

Experimental details

Tables S1 – S4

Figures S1 – S17

References

Experimental details

Abbreviations used: BEA (but-3-en-1-ammonium), BEA-I₂ (3,4-diiodobutan-1-ammonium), BEA-Br₂ (3,4-dibromobutan-1-ammonium), BEA-Cl₂ (3,4-dichlorobutan-1-ammonium), and MA (methylammonium). Aqueous solutions were prepared using deionized water. Organic solvents were of reagent grade or higher purity and were not dried prior to use except for *N,N*-dimethylformamide (DMF), which was dried and degassed using a JC Meyer solvent purification system. The perovskites (BEA)₂[PbBr₄] and (PEA)₂[CuCl₄] were synthesized according to our previous report.¹ All other reagents were purchased from commercial vendors and used as received. Prior to the halogenation reactions, the 2D perovskites were ball-milled for 3 h at 500 rpm in 12-mL zirconia vials equipped with 5-mm agate balls using a Fritsch Pulverisette 7 planetary mill.

Cleaning FTO substrates

All 3D perovskite films were deposited on fluorine-doped tin oxide (FTO) coated glass slides (15 Ωsq⁻¹ sheet resistance) to prevent charging during SEM imaging. Large FTO substrates were cut into 1.5 × 1.5 cm² squares and then sequentially cleaned with *Extran*® detergent, acetone, and isopropanol. During each step, the substrates were fully submerged in an ultrasonic bath for 10 minutes. After the final isopropanol wash, the wet substrates were dried with a high-pressure air line before being placed in a UV-ozone cleaner for 20 minutes.

Independent preparation of (MA)[PbX₃] films (X = Cl and Br)

To compare against the quality of films formed from (MA)[PbI₃] and Br₂ or Cl₂ gas, (MA)[PbBr₃] and (MA)[PbCl₃] films were independently prepared using a method similar to that used for (MA)[PbI₃] films. A 0.5-M PbBr₂ (183 mg, 0.500 mmol) or PbCl₂ (139 mg, 0.500 mmol) DMF solution (1 mL) was spun onto clean FTO substrates. This film was converted into the perovskite through the dropwise addition of a 10 mg/mL (MA)Br solution or (MA)Cl solution in dry isopropanol (1 mL).

Solution-state synthesis of (BEA-Cl₂)₂[PbBr₄]

A solution of (BEA)Cl (0.10 g, 0.93 mmol) in 10 mL of methanol was cooled to 0 °C and bubbled with Cl₂ gas for 2 minutes. The solution was allowed to stir for 1 h in the dark after which all volatiles were removed under reduced pressure. The resulting colorless solid was dissolved in 3 mL of methanol and added dropwise to a stirred, cold (−10 °C), 5-mL solution of PbBr₂ (0.17 g, 0.46 mmol) in 9-M HBr. After 10 minutes, the resulting colorless precipitate was filtered while cold through a glass frit and washed with cold (−10 °C) diethyl ether (2 × 5 mL). The colorless crystalline solid was held at reduced pressure for 1 h to afford 0.303 g (81.0% yield) of product. Crystals suitable for single-crystal x-ray diffraction were obtained by slow evaporation of a concentrated solution of (BEA-Cl₂)₂[PbCl₄] in 12-M HCl. IR(neat): 3007(s), 2910(s), 1575(w), 1465(s), 1386(w), 1125(m), 995(m), 923(s), 773(s), and 629(w) cm⁻¹. Anal. Calcd. for C₈H₂₀N₂PbCl₈: C, 15.13; H, 3.17; N, 4.41. Found: C, 15.10; H, 3.02; N, 4.33.

Characterization of the solid-state reaction product of (BEA)₂[PbBr₄] and Br₂: (BEA-Br₂)₂[PbBr₄]

IR(neat): 3091(s), 3015(s), 2910(s), 1572(m), 1477(s), 1426(s), 1401(m), 1328(w), 1206(w), 1158(s), 1129(w), 1094(s), 1065(m), 1028(m), 987(w), 933(s), 878(w), 787(s), 712(m), 644(m), and 565(s) cm⁻¹. The PXRD pattern is shown in Figure S1. Crystals suitable for single-crystal diffraction studies were obtained by slow evaporation of a filtered, concentrated solution of (BEA-Br₂)₂[PbBr₄] in a 1:1 methanol:HBr (9 M) mixture.

Characterization of the solid-state reaction product of (PEA)₂[CuCl₄] and Br₂: (PEA-Br₂)₂[CuCl₄]

IR(neat): 3087(s), 3019(s), 2932(s), 1567(m), 1481(s), 1429(m), 1392(w), 1325(m), 1223(w), 1159(m), 1090(m), 1058(w), 951(m), 884(s), 718(m), 646(m), and 579(s) cm⁻¹. The PXRD pattern is shown in Figure S6. Crystalline (PEA-Br₂)₂[CuCl₄] was independently synthesized by stirring 1 mL of a 0.25-M methanol solution of (PEA)Cl with 1.2 equivalents of Br₂, 0.1 mL of 12-M HCl, and 2 mL of methanol. The solution was stirred for 2 h and then 0.5 mL of a 0.25-M solution of CuCl₂ in methanol was added. Slow solvent evaporation yielded yellow plate-like crystals of (PEA-Br₂)₂[CuCl₄] after 4 days.

Characterization of the solid-state reaction product of (BEA)₂[PbBr₄] and Cl₂: (BEA-Br₂)₂[PbCl₄]

IR(neat): 3093(s), 3002(s), 2921(s), 1594(m), 1490(s), 1428(w), 1403(m), 1303(w), 1207(m), 1160(s), 1128(m), 1097(m), 1064(m), 1035(m), 985(w), 952(m), 790(s), 715(m), 642(m), and 559(s) cm⁻¹. The PXRD pattern is shown in Figure S10. Crystals suitable for single-crystal diffraction studies were obtained by slow evaporation of a filtered, concentrated solution of (BEA-Br₂)₂[PbCl₄] in 12-M HCl.

General procedure for I₂-Br₂ gas separation

Solid samples of (BEA)₂[PbBr₄] (2–3 mg) and solid I₂ (0.5 g) were introduced into a gas-tight chamber of known volume. The chamber was allowed to equilibrate for 15–30 minutes, and then a known volume of Br₂-saturated air was quickly injected into the chamber ensuring that the molar quantity of (BEA)₂[PbBr₄] were at least two times that of the injected Br₂. After 12 h the solid was removed from the chamber and held at reduced pressure for 0.5 h to remove surface-adsorbed Br₂ or I₂. The solid was then dissolved in *d*⁶-DMSO and analyzed by ¹H NMR. The results of these experiments are shown in Table S1.

Table S1. Percentage of bromine captured from iodine-bromine mixtures

Sample	Br ₂ : I ₂ Ratio	% of Br ₂ captured by the perovskite
1	1: 1	88
2	1: 1	85
3	1: 2	82
4	1: 2	87
5	1: 2	89

Powder x-ray diffraction (Powder XRD)

Experiments were conducted on a Panalytical X'Pert Pro diffractometer with a Bragg-Brentano geometry and PIXCEL 1D detector equipped with a nickel filter. Experimental conditions are given in Table S2. The simulated powder patterns were calculated using the crystallographic information files (CIFs) from single-crystal x-ray experiments.

Table S2. Experimental details for powder x-ray diffraction experiments

Step size (° 2Theta)	0.02
Divergence slit type	Automatic
Anode material	Cu
K α_1 (Å)	1.54060
K α_2 (Å)	1.54443
K α_2 / K α_1 ratio	0.50000

Other physical measurements

Infrared spectra were collected on a Thermo Nicolet 6700 spectrometer with a Smart Orbit attenuated total reflectance accessory. NMR spectra were recorded on a Varian Inova-500 instrument and peaks were referenced to residual solvent peaks. Carbon, hydrogen, and nitrogen analyses were obtained from MHW Laboratories (Phoenix, AZ). Mass spectrometry in methanol was performed in a Waters 2795 HPLC system ZQ single quadrupole MS with an electrospray ionization source using direct injection. SEM images were collected on an FEI XL30 Sirion SEM with an FEG source. Images were collected with a voltage of 5 kV and a beam current of 71 pA.

Crystal structure determination

Crystals were coated with Paratone-N oil, attached to a Kapton loop, and transferred to a Bruker D8 Venture diffractometer equipped with a Photon 100 CMOS detector or to the Bruker D8 diffractometer at the Advanced Light Source beamline 11.3.1 at the Lawrence Berkeley National Laboratory. Frames were collected using ω and ψ scans and the unit-cell parameters were refined against all data. The crystals did not show significant decay during data collection. Data were integrated and corrected for Lorentz and polarization effects using SAINT 8.27b, and were corrected for absorption effects using SADABS V2012.² Space-group assignments were based upon systematic absences, *E*-statistics, agreement factors for equivalent reflections, and successful refinement of the structure. The structures were solved by direct methods and expanded through successive difference Fourier maps using SHELXS-97. They were refined against all data using the SHELXTL-2013 software package.^{3,4} Hydrogen atoms were inserted at idealized positions and refined using a riding model with an isotropic thermal parameter 1.2 times that of the attached carbon atom or 1.5 times that of the attached nitrogen. Thermal parameters for all non-hydrogen atoms were refined anisotropically. The disorder in (BEA-Br₂)₂[PbCl₄] was modeled using similarity restraints on 1,2- and 1,3-distances as well as rigid-bond restraints for anisotropic displacement parameters. The occupancies of disordered groups were allowed to refine freely, while constraining the sum of the occupancies to unity. Similar rigid-bond restraints were also applied to atoms not involved in the disorder to stabilize the refinement. Details regarding the data quality and a summary of the residual values of the refinements are listed in Tables S3 and S4.

Structural models of (PEA)₂[CuCl₄] and (PEA-Br₂)₂[CuCl₄]

Crystals of (PEA)₂[CuCl₄] and (PEA-Br₂)₂[CuCl₄] were heavily twinned and despite several efforts we were unable to obtain a high-quality structure. The data quality, however, is enough to corroborate the overall layered perovskite structure for both materials and show that the PEA molecules are oxidized to form the brominated product: PEA-Br₂.

Table S3. Crystallographic data for (BEA-Br₂)₂[PbBr₄] and (BEA-Cl₂)₂[PbBr₄]

	(BEA-Br ₂) ₂ [PbBr ₄]	(BEA-Cl ₂) ₂ [PbBr ₄]
Empirical formula	C ₈ H ₂₀ Br ₈ N ₂ Pb	C ₈ H ₂₀ Br ₄ Cl ₄ N ₂ Pb
Formula weight, g mol ⁻¹	990.73	812.89
Temperature, K	100(2)	100(2)
Wavelength, Å	0.71073	0.6888
Crystal system	Triclinic	Triclinic
Space group	<i>P</i> -1	<i>P</i> -1
<i>a</i> , Å	7.973(1)	7.792(3)
<i>b</i> , Å	8.388(1)	8.315(3)
<i>c</i> , Å	16.775(2)	16.462(6)
α , °	95.61(1)	97.337(5)
β , °	95.89(1)	96.252(5)
γ , °	90.37(1)	90.184(4)
Volume, Å ³	1110.5(2)	1051.4(7)
<i>Z</i>	2	2
Density (calculated), g cm ⁻³	2.963	2.568
Absorption coefficient, mm ⁻¹	21.980	14.83
<i>F</i> (000)	888	744
Crystal size, mm ³	0.04 × 0.04 × 0.02	0.12 × 0.10 × 0.02
Theta range, °	2.44 to 25.35	2.7 to 24.8
Index ranges	-9 ≤ <i>h</i> ≤ 8 -10 ≤ <i>k</i> ≤ 10 -20 ≤ <i>l</i> ≤ 20	-9 ≤ <i>h</i> ≤ 9 -10 ≤ <i>k</i> ≤ 10 -20 ≤ <i>l</i> ≤ 20
Reflections collected/unique	19723 / 4067	9611 / 3982
Completeness to theta max, %	100	99.7
Max. and min. transmission	0.668 and 0.473	0.159 and 0.264
Data / restraints / parameters	4067 / 106 / 177	3982 / 0 / 177
Goodness-of-fit on <i>F</i> ²	1.051	1.03
Final <i>R</i> indices [<i>I</i> > 2σ(<i>I</i>)] ^a	<i>R</i> ₁ = 0.0593 w <i>R</i> ₂ = 0.0868	<i>R</i> ₁ = 0.040 w <i>R</i> ₂ = 0.052
<i>R</i> indices (all data) ^a	<i>R</i> ₁ = 0.059 w <i>R</i> ₂ = 0.110	<i>R</i> ₁ = 0.046 w <i>R</i> ₂ = 0.108
Largest diff. peak and hole, e Å ⁻³	1.10 and -1.70	1.94 and -1.84

$$^a R_1 = \frac{\sum ||F_o| - |F_c||}{\sum |F_o|}, \quad wR_2 = \frac{[\sum w(F_o^2 - F_c^2)^2 / \sum (F_o^2)^2]}{1/2}$$

Table S4. Crystallographic data for (BEA-Br₂)₂[PbCl₄]
(BEA-Br₂)₂[PbCl₄]

Empirical formula	C ₈ H ₂₀ Br ₄ N ₂ PbCl ₄
Formula weight, g mol ⁻¹	1009.92
Temperature, K	200(2)
Wavelength, Å	0.6888
Crystal system	Monoclinic
Space group	<i>P</i> 2 ₁ / <i>c</i>
<i>a</i> , Å	5.416(1)
<i>b</i> , Å	5.444(1)
<i>c</i> , Å	35.809(4)
α , °	90
β , °	93.365(1)
γ , °	90
Volume, Å ³	1053.9(2)
<i>Z</i>	2
Density (calculated), g cm ⁻³	3.182
Absorption coefficient, mm ⁻¹	22.10
<i>F</i> (000)	880
Crystal size, mm ³	0.2 × 0.15 × 0.05
Theta range, °	3.4 to 28.7
Index ranges	-7 ≤ <i>h</i> ≤ 7 -7 ≤ <i>k</i> ≤ 7 -48 ≤ <i>l</i> ≤ 48
Reflections collected/unique	25379 / 2736
Completeness to theta max, %	100
Max. and min. transmission	0.450 and 0.670
Data / restraints / parameters	2736 / 155 / 174
Goodness-of-fit on <i>F</i> ²	1.21
Final <i>R</i> indices	<i>R</i> ₁ = 0.040
[<i>I</i> > 2σ(<i>I</i>)] ^a	w <i>R</i> ₂ = 0.076
<i>R</i> indices (all data) ^a	<i>R</i> ₁ = 0.059 w <i>R</i> ₂ = 0.112
Largest diff. peak and hole, e Å ⁻³	1.84 and -2.47

$$^a R_1 = \frac{\sum ||F_o| - |F_c||}{\sum |F_o|}, \quad wR_2 = \left[\frac{\sum w(F_o^2 - F_c^2)^2}{\sum (F_o^2)^2} \right]^{1/2}$$

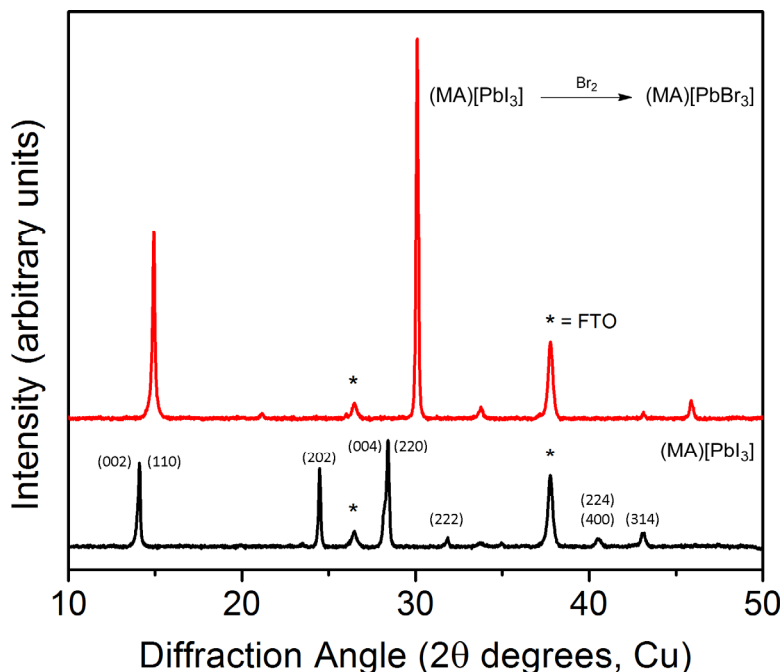


Figure S1. Powder XRD patterns of a (MA)[PbI₃] film before (black) and after reaction with Br₂ vapor to form (MA)[PbBr₃] (red). The intensity of the reflections in the XRD pattern typically increases from this process. Reflections corresponding to FTO are marked with asterisks. The (MA)[PbI₃] reflections are indexed according to the tetragonal structure.

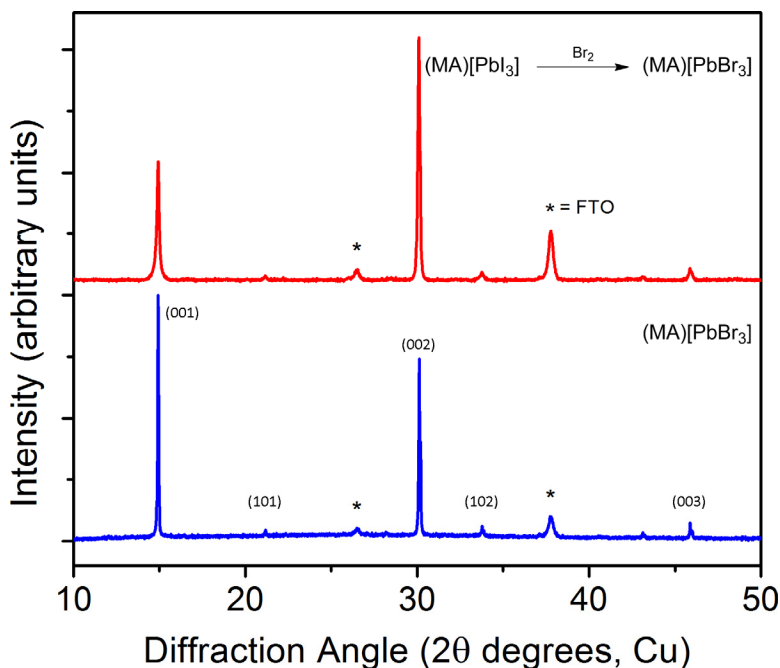


Figure S2. Powder XRD patterns of independently synthesized (MA)[PbBr₃] (blue) and (MA)[PbBr₃] formed through reaction of (MA)[PbI₃] and Br₂ (red). Reflections corresponding to FTO are marked with asterisks. The (MA)[PbBr₃] reflections are indexed according to the cubic structure.

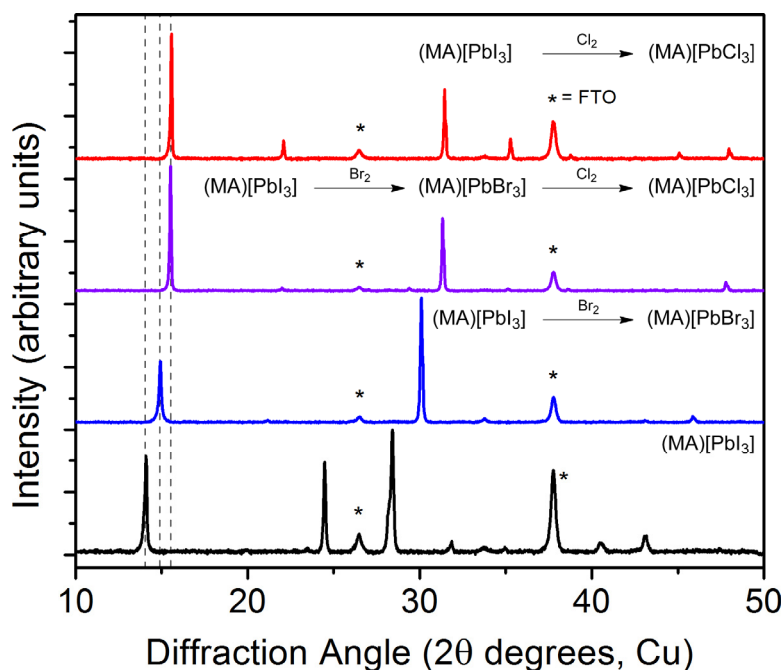


Figure S3. Powder XRD patterns of films of (MA)[PbI₃] (black), and of these films after reaction with Br₂ vapor (blue), sequential reaction with Br₂ and then Cl₂ vapor (purple), and reaction with Cl₂ vapor (red). Reflections corresponding to the FTO substrate are marked with asterisks.

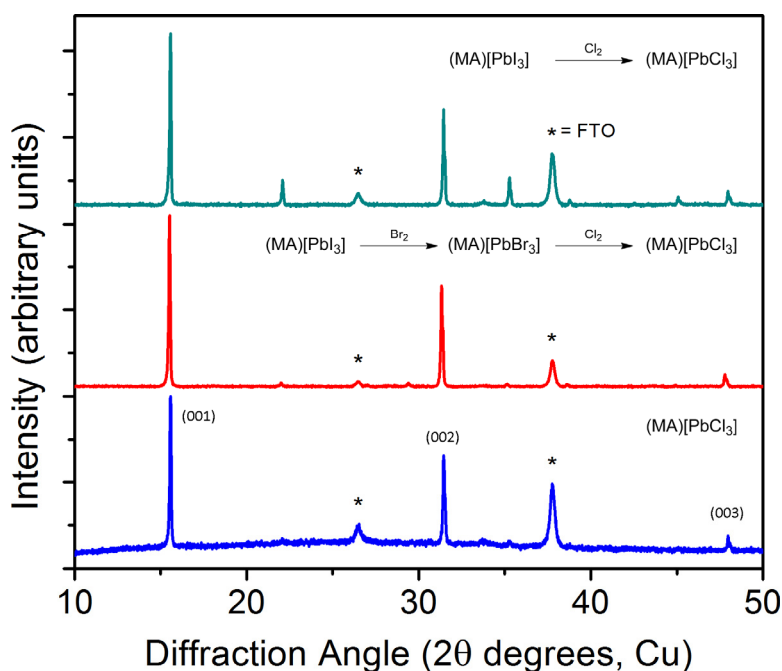


Figure S4. Powder XRD patterns of independently synthesized (MA)[PbCl₃] (blue), (MA)[PbCl₃] formed through sequential reaction of (MA)[PbI₃] with Br₂ and Cl₂ (red), and (MA)[PbCl₃] formed through reaction of (MA)[PbI₃] with Cl₂ (cyan). Reflections corresponding to FTO are marked with asterisks. The (MA)[PbCl₃] reflections are indexed according to the cubic structure.

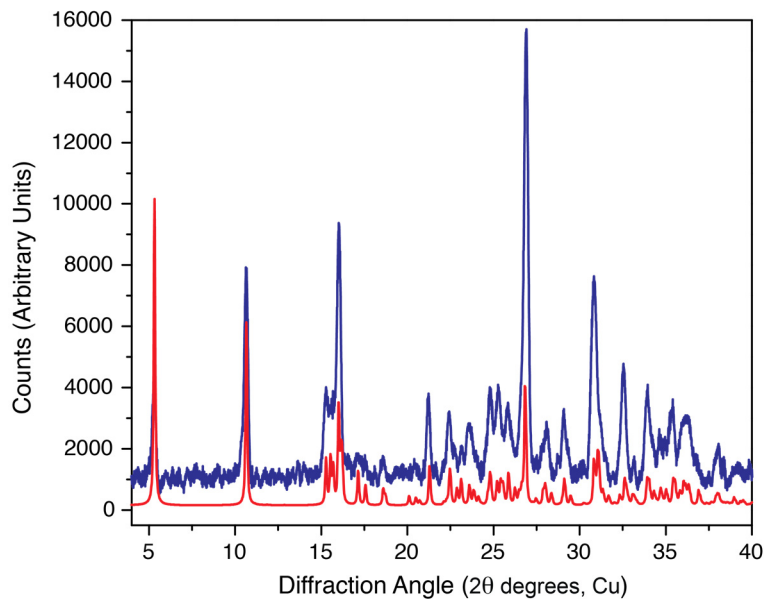


Figure S5. Powder XRD patterns of $(\text{BEA-Br}_2)_2[\text{PbBr}_4]$ obtained by the reaction of Br_2 vapor and $(\text{BEA})_2[\text{PbBr}_4]$ (blue) and the simulated powder pattern from the single-crystal structure of $(\text{BEA-Br}_2)_2[\text{PbBr}_4]$ (red).

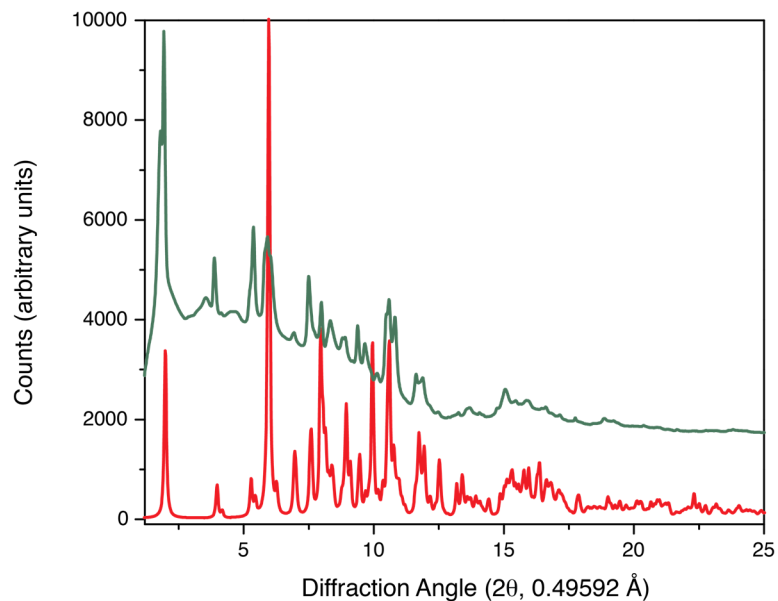


Figure S6. Powder XRD patterns of $(\text{PEA-Br}_2)_2[\text{CuCl}_4]$ obtained by the reaction of Br_2 vapor and $(\text{PEA})_2[\text{CuCl}_4]$ (green) and the simulated powder pattern from the model crystal structure of $(\text{PEA-Br}_2)_2[\text{CuCl}_4]$ (red).

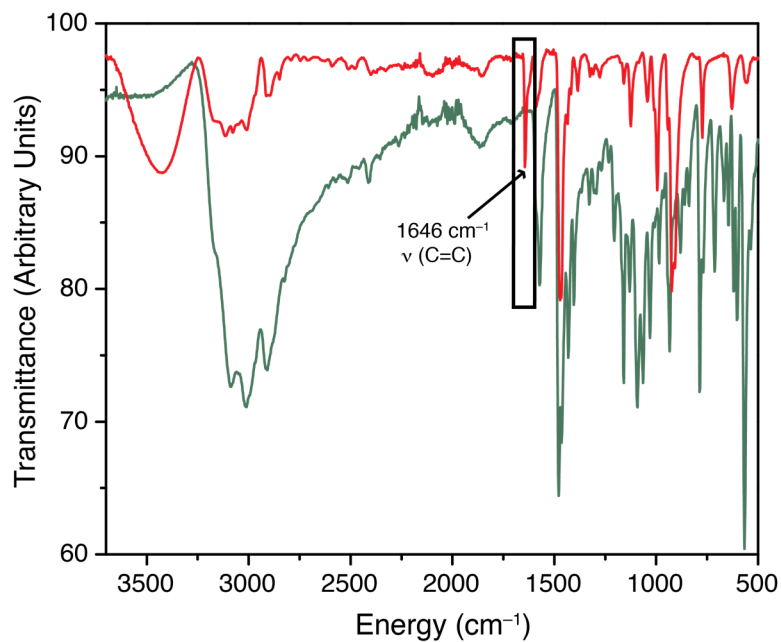


Figure S7. Solid-state vibrational spectra of (BEA)₂[PbBr₄] (red) and (BEA-Br₂)₂[PbBr₄] (green) obtained by the reaction of Br₂ vapor with (BEA)₂[PbBr₄]. The alkene C=C stretch in (BEA)₂[PbBr₄] is highlighted.

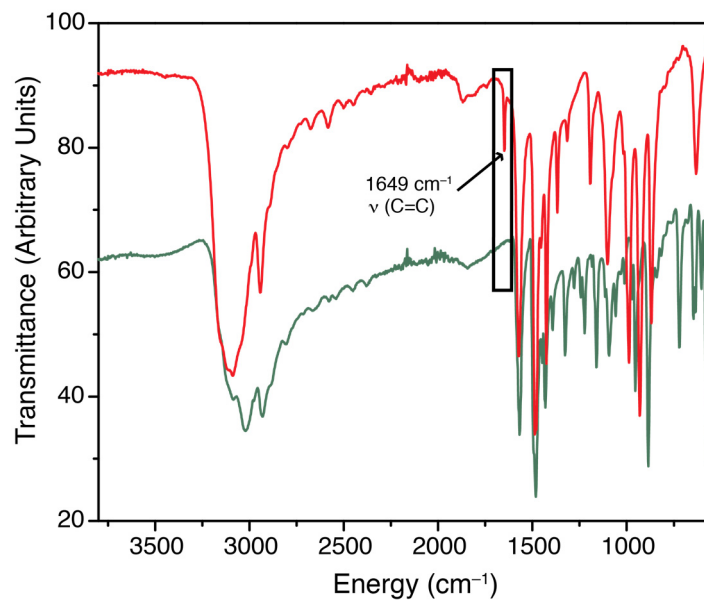


Figure S8. Solid-state vibrational spectra of (PEA)₂[CuCl₄] (red) and (PEA-Br₂)₂[CuCl₄] (green). The alkene C=C stretch in (PEA)₂[CuCl₄] is highlighted.

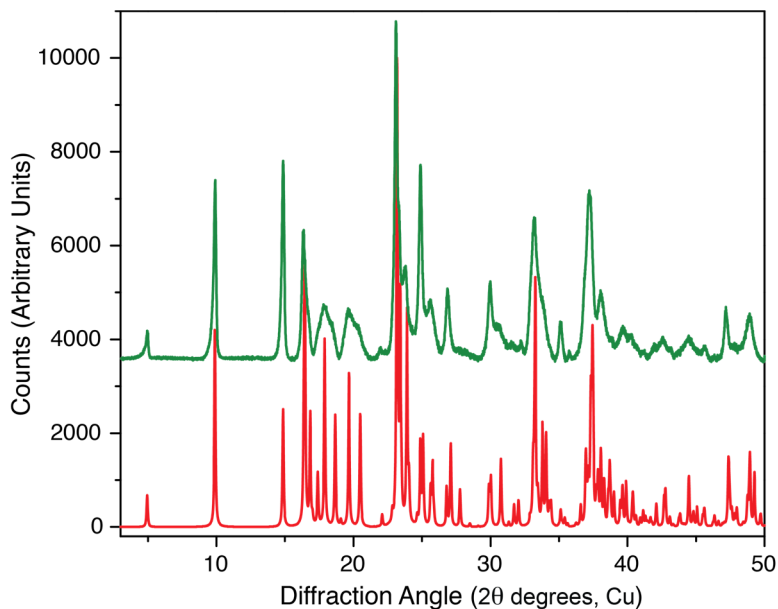


Figure S9. Powder XRD patterns of $(\text{BEA-Br}_2)_2[\text{PbCl}_4]$ obtained by the reaction of Cl_2 vapor and $(\text{BEA})_2[\text{PbBr}_4]$ (green) and the simulated powder pattern from the single-crystal structure of $(\text{BEA-Br}_2)_2[\text{PbCl}_4]$ (red).

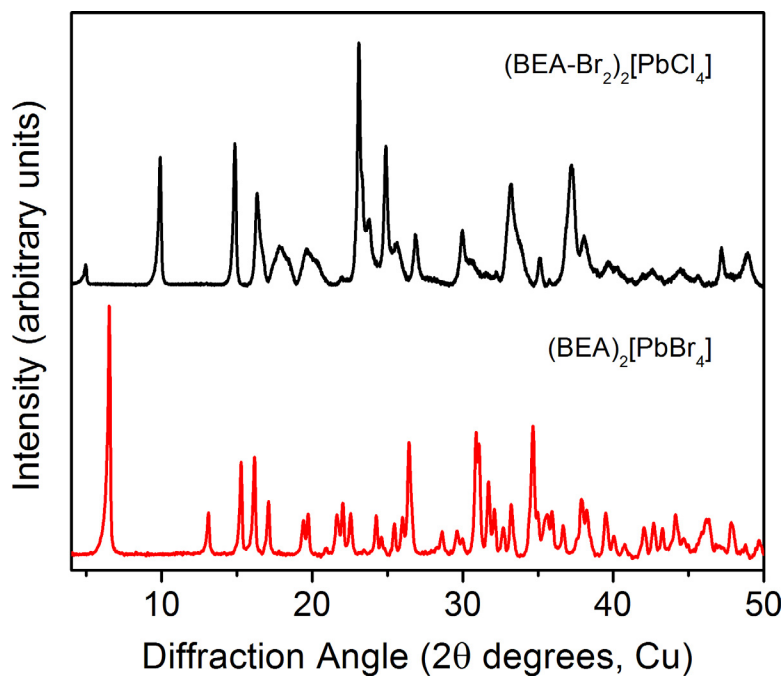


Figure S10. Powder XRD patterns of $(\text{BEA})_2[\text{PbBr}_4]$ (red) and $(\text{BEA-Br}_2)_2[\text{PbCl}_4]$ (black) obtained from the reaction of $(\text{BEA})[\text{PbBr}_4]$ with Cl_2 .

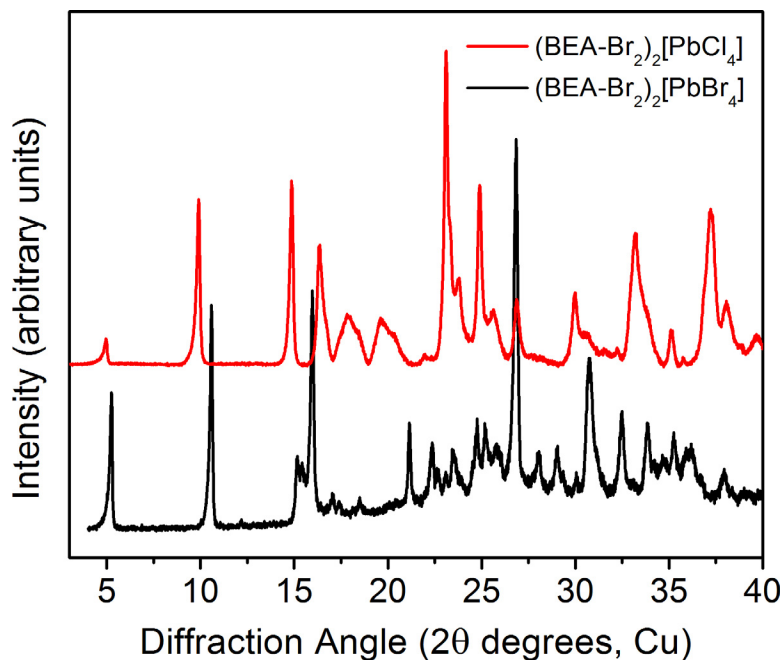


Figure S11. Powder XRD patterns of $(\text{BEA-Br}_2)_2[\text{PbBr}_4]$ (black) and $(\text{BEA-Br}_2)_2[\text{PbCl}_4]$ obtained through the reaction of $(\text{BEA-Br}_2)_2[\text{PbBr}_4]$ with Cl_2 (red).

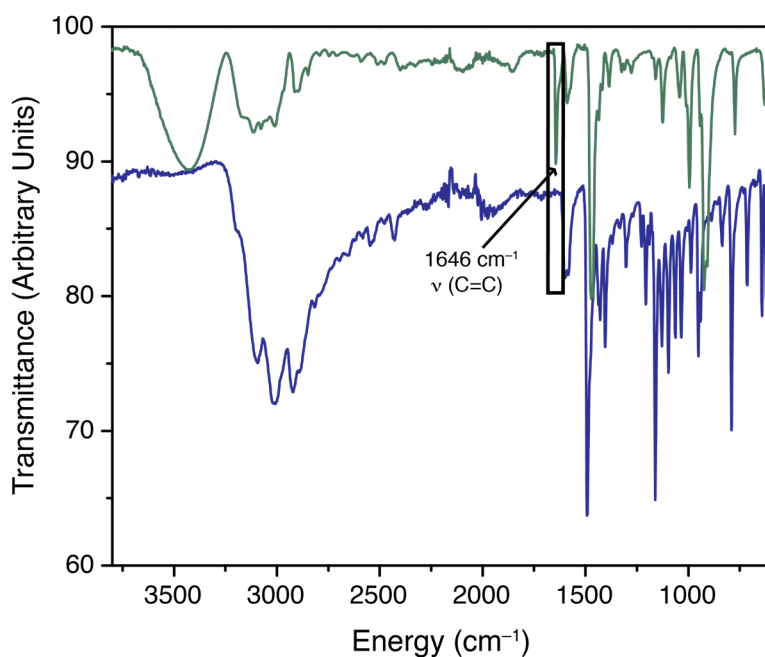


Figure S12. Solid-state vibrational spectra of $(\text{BEA})_2[\text{PbBr}_4]$ (green) and $(\text{BEA-Br}_2)_2[\text{PbCl}_4]$ (blue) obtained by the reaction of Cl_2 gas with $(\text{BEA})_2[\text{PbBr}_4]$. The alkene $\text{C}=\text{C}$ stretch in $(\text{BEA})_2[\text{PbBr}_4]$ is highlighted.

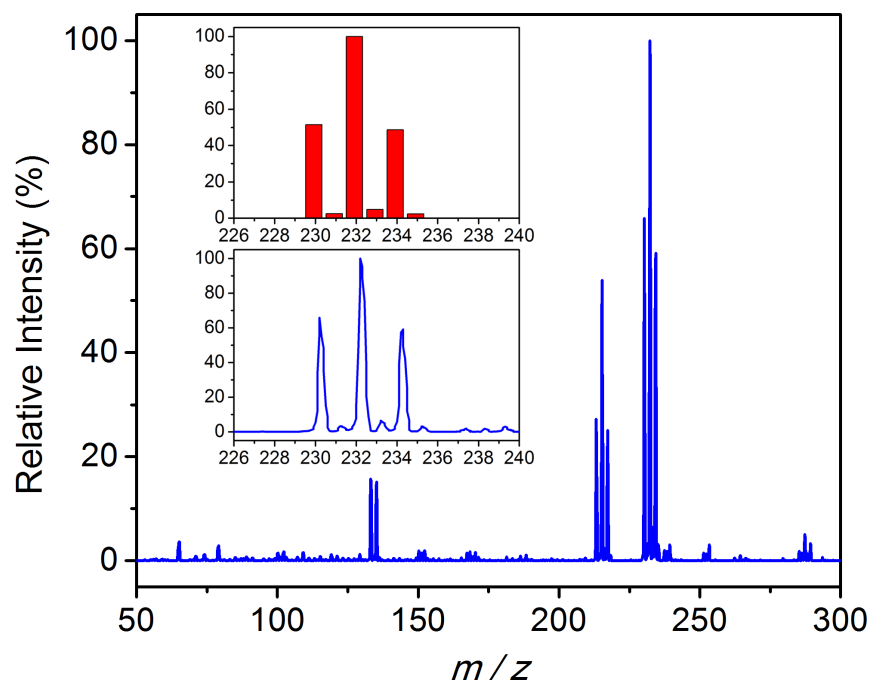


Figure S13. Mass spectrum of the organic products obtained from the reaction of $(\text{BEA})_2[\text{PbBr}_4]$ and Br_2 vapor. Inset: simulated mass spectrum for BEA-Br_2 (red) and a close-up of the experimental spectrum (blue). The peak at $215 m/z$ is assigned to a fragment formed through loss of NH_3 from BEA-Br_2 during the measurement.

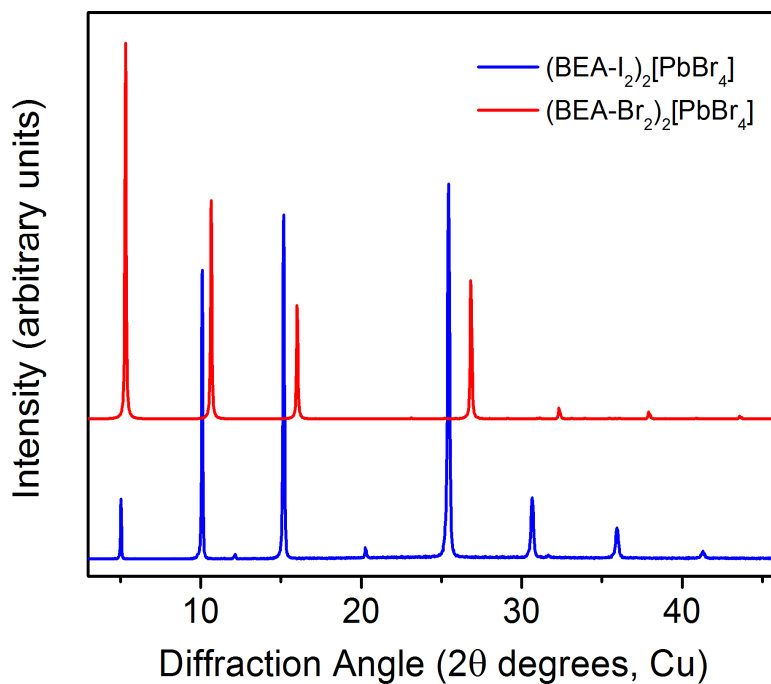


Figure S14. Powder XRD patterns of $(\text{BEA-I}_2)_2[\text{PbBr}_4]$ (blue) and $(\text{BEA-Br}_2)_2[\text{PbBr}_4]$ (red) obtained through reaction of $(\text{BEA})_2[\text{PbBr}_4]$ with I_2 and Br_2 vapor, respectively.

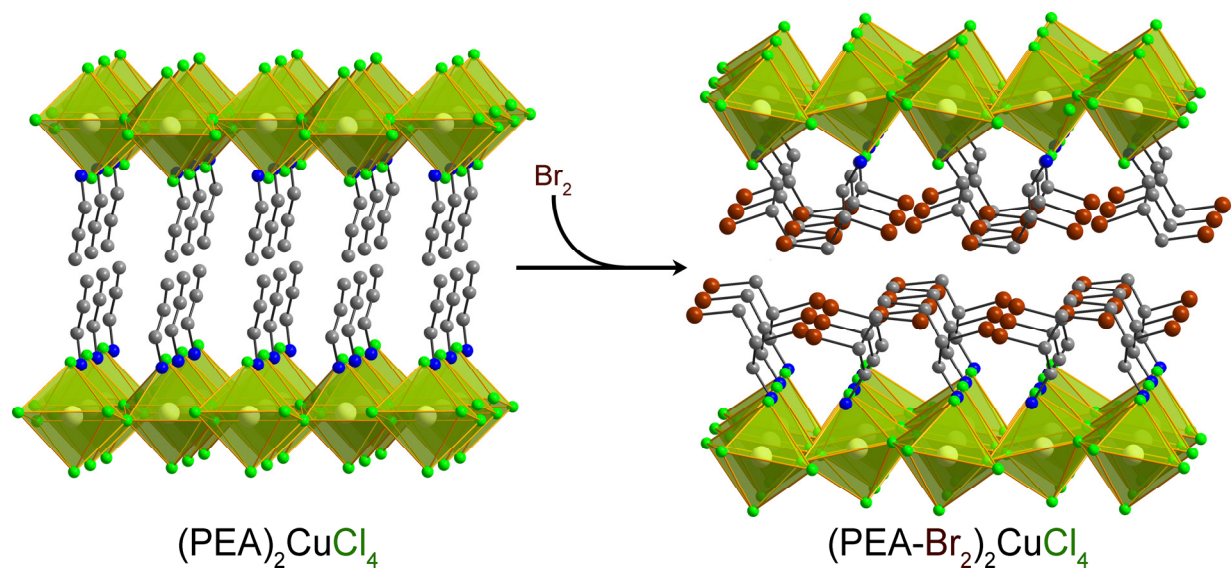


Figure S15. Reaction of $(\text{PEA})_2[\text{CuCl}_4]$ with Br_2 gas. Structural models of $(\text{PEA})_2[\text{CuCl}_4]$ and $(\text{PEA-Br}_2)_2[\text{CuCl}_4]$. Cu–Cl octahedra: green, Cu: yellow, Br: brown, Cl: green, N: blue, C: gray. Hydrogen atoms are omitted for clarity.

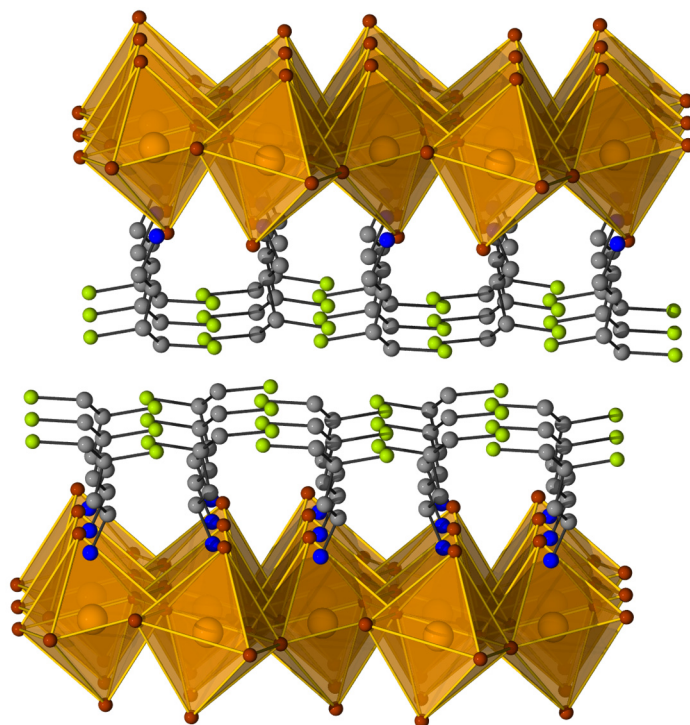


Figure S16. Crystal structure of $(\text{BEA-Cl}_2)_2[\text{PbBr}_4]$. Pb–Br octahedra: orange, Pb: orange, Br: brown, Cl: green, N: blue, C: gray. Hydrogen atoms are omitted for clarity.

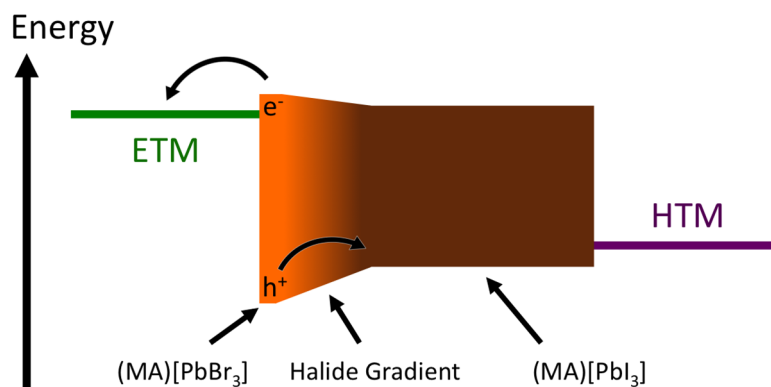


Figure S17. Band level diagram for a hypothetical photovoltaic device using a Pb–Br and a Pb–I perovskite absorber with a halide gradient at the Pb–I/Pb–Br interface. The slope of the bandgap at the interface could shuttle holes towards the cathode. Band levels were obtained from literature reports.⁵ ETM: electron transport material, HTM: hole transport material.

References

- [1] Solis-Ibarra, D., & Karunadasa, H. I. *Angew. Chem. Int. Ed.* **2014**, *53*(4), 1039–1042.
- [2] SAINT and SADABS; Bruker AXS Inc.: Madison, WI, (2007).
- [3] Sheldrick, G. M. *SHELXL-97, Program for crystal structure refinement*; Göttingen, **1997**.
- [4] G. M. Sheldrick, G. M. *Acta Cryst. Sect. A* **2008**, *64*, 112–122.
- [5] Schulz, P.; Edri, E.; Kirmayer, S.; Hodes, G.; Cahen, D.; Kahn, A. *Energy Environ. Sci.* **2014**, *7*, 1377–1381.